fire

MDPI

Article

Sensitivity to the Representation of Wind for Wildfire Rate of Spread: Case Studies with the Community Fire Behavior Model

Masih Eghdami *, Pedro A. Jiménez y Muñoz and Amy DeCastro

Research Application Laboratory, NSF National Center for Atmospheric Research, Boulder, CO 80307, USA; jimenez@ucar.edu (P.A.J.y.M.)
* Correspondence: masih@ucar.edu

Abstract: Accurate wildfire spread modeling critically depends on the representation of wind dynamics, which vary with terrain, land cover characteristics, and height above ground. Many fire spread models are often coupled with coarse atmospheric grids that cannot explicitly resolve the vertical variation of wind near flame heights. Rothermel's fire spread model, a widely used parameterization, relies on midflame wind speed to calculate the fire rate of spread. In coupled fire atmosphere models such as the Community Fire Behavior Model (CFBM), users are required to specify the midflame height before running a fire spread simulation. This study evaluates the use of logarithmic interpolation wind adjustment factors (WAF) for improving midflame wind speed estimates, which are critical for the Rothermel model. We compare the fixed wind height approach that is currently used in CFBM with WAF-derived winds for unsheltered and sheltered surface fire spread. For the first time in this context, these simulations are validated against satellite and ground-based observations of fire perimeters. The results show that WAF implementation improves fire perimeter predictions for both grass and canopy fires while reducing the overestimation of fire spread. Moreover, this approach solely depends on the fuel bed depth and estimation of canopy density, enhancing operational efficiency by eliminating the need for users to specify a wind height for simulations.

Keywords: wildland fires; flame length; wind interpolation

Received: 13 February 2025
Revised: 13 March 2025
Accepted: 17 March 2025
Published: 31 March 2025

Citation: Eghdami, M.; Muñoz, P.A.J.y.; DeCastro, A. Sensitivity to the Representation of Wind for Wildfire Rate of Spread: Case Studies with the Community Fire Behavior Model. *Fire* **2025**, *8*, 135. https://doi.org/10.3390/fire8040135

1. Introduction

Wind is the most influential element in the prediction of wildfire spread. The speed and direction of the wind fluctuate over different time scales and are influenced by terrain and land surface cover, which substantially affects the fire dynamics. Wind speed varies vertically with the height above the ground due not only to local surface characteristics, such as surface roughness, but also boundary layer processes and atmospheric stability. Thus, determining the appropriate wind speed for modeling surface fire spread, flame length, and intensity is a complex and crucial endeavor.

Coupled atmosphere and fire behavior models [1–4] have become increasingly popular tools for predicting fire spread and smoke dispersion. Operational atmospheric models often use grid spacing coarser than 1 km due to computational resource limitations. At these scales, the models cannot explicitly resolve fire physics such as combustion. Therefore, fire spread and heat release are often parameterized using semiempirical models. A widely used parameterization in both research and operational applications is Rothermel's surface fire spread model [5]. This model predicts the spread rate based on fuel characteristics, moisture, terrain slope, and wind speed. Rothermel's model uses midflame height wind

speed, which is not explicitly calculated in operational weather models with 1 km scale grid spacing.

Flame length (or height) serves as a critical visual indicator of fire intensity in wildland fire modeling and management [6,7]. Flame length correlations are often used to predict the likelihood of crown fires, which occur when surface fires reach the forest canopy. While various empirical studies have established flame length as a power function of fireline intensity (αI^{β}), the coefficients and exponents in these correlations exhibit considerable variation. This variability can be partly attributed to the lack of standardized methodologies for measuring fluctuating flame length and the subjective nature of estimation methods [7]. Furthermore, although empirical flame length models account for spread rate, fuel energy, and load, they do not fully incorporate variations in fuel characteristics like moisture, density, compactness, and fuel bed height, making them susceptible to errors.

Modeling midflame wind speed poses challenges, especially near or within canopies. Operational Numerical Weather Prediction (NWP) models predict wind at meteorological standard heights (e.g., 10 m) rather than directly at the surface, and generally lack the vertical resolution required to capture wind profiles in these areas (e.g., [4,8,9]). Furthermore, complex factors like variable foliage density, canopy height, and tree arrangement add difficulty to accurate wind representation. Sub-canopy jets and secondary wind maxima, which can influence fire spread prediction, are often overlooked by simplified models. Terrain features, such as slopes and canyons, further complicate this modeling, demanding high spatial resolution with computationally intensive simulations. Finally, limited observational data for model validation and input remains a critical constraint.

In this study, we examined sensitivities to the representation of the winds driving the fire rate of spread using the Community Fire Behavior model (CFBM, version 0.2.0 [10]). CFBM closely follows the Weather Research and Forecasting Fire module (WRF-Fire) [2,3], which is widely used to simulate wildfire–atmosphere interactions (WRF, [11]). The flame length is diagnosed in the model based on Byram's fireline intensity [12] but is not used for calculating the midflame height wind. Instead, fire wind height is constant throughout the domain and needs to be specified by the user. The default value of this parameter is 1 m, which is too high for some grass fires. Furthermore, for sheltered (canopy) fires, this may lead to unrealistic results, as the atmospheric roughness length is of a similar order of magnitude. The wind used for fire spread is interpolated to midflame height assuming a logarithmic profile with surface roughness length scale used in the atmospheric model.

Incorporating improved canopy wind models into coupled fire–atmosphere systems like WRF-SFIRE (a variation of WRF-Fire) has demonstrated substantial improvements in simulating fire spread rates, particularly when sub-canopy wind dynamics are important [13,14]. For instance, the implementation of an improved canopy model (ICM; [14,15]) into WRF-SFIRE accounts for the vertical structure of foliage density of forest canopies. Their results demonstrated that incorporating an ICM led to more realistic sub-canopy wind speeds, aligning better with observations taken from a network of anemometers positioned throughout the forest. Improved wind speed prediction led to more accurate fire spread rates, improving the predictions by approximately a factor of two compared to configurations relying solely on logarithmic profiles. Furthermore, the enhanced canopy model provided better smoke representation in the simulations. More recently [13], ICM models have been validated using horizontal wind speed measurements from flux tower sites, further confirming their ability to improve wildfire spread and intensity predictions by resolving critical sub-grid wind variations within forest canopies.

For this study, we aimed to simplify the subjective decision of determining fire wind height by employing a model commonly used in field operations, such as BehavePlus and Fire Area Simulator (FARSITE). This approach uses a wind adjustment factor (WAF) based

on a logarithmic wind profile that depends only on the fuel bed depth and, in the case of sheltered fire, canopy density [16,17]. The WAF was originally formulated to diagnose the midflame height required by the Rothermel model, which makes it directly applicable to both WRF-Fire and CFBM since they use the Rothermel model for fire spread. The wind adjustment factor for 10-m wind typically ranges between 0.5 for unsheltered exposed fuel to 0.1 for sheltered fuel with dense canopy cover. While the WAF model simplifies the process, users still need to determine whether the fire is burning in a sheltered or unsheltered environment to select the appropriate WAF value. For this study, simulations were conducted for selected cases covering two unsheltered grass fires and two canopy-sheltered surface fires with a control simulation using a constant midflame height. The model performance was evaluated against perimeter observations from the National Interagency Fire Center (NIFC, https://data-nifc.opendata.arcgis.com, accessed on 21 May 2024) and active fire detections from Visible Infrared Imaging Radiometer Suite (VIIRS, [18]).

2. Numerical Model and Wind Adjustment Factor

2.1. Numerical Simulations

We used the WRF model version 4.3.3 to produce atmospheric fields required as input for the CFBM. For the WRF simulations, the initial and boundary conditions were extracted from High-Resolution Rapid Refresh (HRRR [19]), with boundary conditions provided at a 3-h frequency. The WRF domain included a 208 × 208 grid with 1 km grid spacing. The domain had 81 vertical levels, with the model top set at 50 hPa. The physics options included the Thompson and Eidhammer microphysics parameterization [20], the revised MM5 surface layer scheme [21], the Rapid Radiative Transfer Model (RRTMG) longwave [22], the Dudhia shortwave radiation [23] schemes, and the unified Noah land-surface model [24].

We ran the CFBM simulations using a smaller domain of 1000 × 1000 grid points with 100 m grid spacing, centered over the ignition point. The CFBM relies on atmospheric inputs from WRF provided at 15-min intervals. The simulations used the Anderson 13-fuel classifications obtained from LANDFIRE, available at 30 m resolution. The atmospheric fields required for the CFBM control runs included three-dimensional winds, geopotential height, and roughness length. The atmospheric fields necessary for running CFBM with the WAF implementation only require the 10-m wind. The WAF parameterization [25] is explained in Section 2.2.

2.2. Wind Adjustment Factor

The WAF is a key element in Rothermel's surface fire spread model, designed to adjust the wind from a standard wind speed (typically measured 10 m above the bare ground) to the midflame wind speed, which determines the surface fire spread. The adjustment involves assuming a logarithmic wind profile:

$$U_z = \frac{U_*}{\kappa}\, ln\left(\frac{z - D_0}{z_0}\right) \quad (1)$$

where U_z is average wind speed at height z, U_* is the friction velocity, $\kappa = 0.4$ is the von Karman constant, z is height above ground, D_0 is zero-plane displacement height, and z_0 is roughness length. Values for D_0 and z_0 can be estimated based on the vegetation (or fuel bed depth) height H, with $D_0 = 0.64H$ and $z_0 = 0.13H$.

The WAF is calculated differently for sheltered and unsheltered fire spread depending on whether overstory vegetation, such as a tree canopy, is present.

2.2.1. Unsheltered Fuels

These are surface fuels exposed directly to the wind, without the obstruction of an overstory. As a result, the wind speed at the midflame height is higher than in sheltered conditions. The WAF is greater in this case, allowing for a closer match between the midflame wind and the 10-m wind speed. In the case of unsheltered fuels, the WAF calculation is based solely on the fuel bed depth and assumes that the wind profile is logarithmic, with the wind speed decreasing as it approaches the surface. The WAF for interpolating wind for unsheltered fuels at height z, based on Equation (1) after substituting D_0 and z_0, is given as:

$$U_H/U_{H+z} = 1/ln\left(\frac{z+0.36H}{0.13H}\right) \tag{2}$$

Now the average wind speed for $H < z < H + H_f$ over the fuel and flame height is the following:

$$WAF = U/U_{10+H} = \left(\frac{1.0+0.36H/H_f}{\ln((10+0.36H)/0.13H)}\right)\left[\ln\left(\frac{H_f/H+0.36}{0.13}\right)-1\right] \tag{3}$$

Note that for this calculation, we need to know the flame height H_F, which is diagnosed using Byram's empirical equation. A simplifying assumption where $H_f = H$ will result in the following:

$$WAF = \overline{U}/U_{10+H} = \left(\frac{1.86}{\ln((10+0.36H)/0.13H)}\right) \tag{4}$$

2.2.2. Sheltered Fuels

For fire spread in surface fuels that are protected from the wind by overstory vegetation, the wind speed is significantly reduced within and below the canopy because the tree crowns block and slow down the wind. We further assume that the wind profile is constant within the canopy area. The wind reduction factor within the canopy is obtained from the following:

$$U_C/U_H = 0.555/\sqrt{fH} \tag{5}$$

where U_C is the wind speed within the canopy, U_H is the wind speed at the top of the canopy and f is a function of canopy density. Combining Equations (2) and (5) will result in the following:

$$WAF = U_C/U_{H+10} = 0.555/\left(\sqrt{fH}\,ln((10+0.36H)/0.13H)\right) \tag{6}$$

For realistic canopy height and density, the WAF for sheltered fires generally ranges from about 0.1 to 0.2 and may approach 0.3 for partially sheltered canopies [25]. Due to limited data on the canopy height and density, we adopt a constant number in our experiments. Note that Equation (6) is based on the 10-m wind above the top of the canopy. In our approach, the wind speed at the top of the canopy is assumed to be the 10-m wind, which is interpolated using the surface roughness for the forested area.

3. Case Selection and Observations

3.1. Fire Case Selection

To ensure this study captures both sheltered (grass) and unsheltered (understory) fires under relevant conditions, we subset the observed fire perimeters using forest and grass masks within the state of Colorado, cross-referenced with VIIRS satellite imagery. The selected fires also included multiple active fire observations within a 48-h window to align with the feasible simulation timeframe. Four case studies were selected to test the fire

spread model, representing both grass (unsheltered fire) and understory (sheltered fire) fuel types (see Table 1 for details). These included two fires with grass fuel, characterized by unsheltered fire spread, and two fires with understory fuel, which involved sheltered fire spread. The grass fuel fires—Boone Draw and Murphy—occurred in open environments where direct wind plays a significant role in driving fire spread. In contrast, the understory fires—Indian Valley and Hayden Pass—took place in forested areas, where tree canopies and denser vegetation reduce the wind driving the fire spread. These cases are not completely surface fire spread, and occasional crown fires are observed during the events. Nevertheless, the primary mode of fire spread remains on the surface and sheltered.

Table 1. Summary of wildfire case studies.

Fire Name	Fuel Type	Area (Acres)	Ignition Point	Ignition Time *	Simulation Time *	Perimeter Time *
Boone Draw	Grass	8598	40.654 N 108.566 W	2018-09-13 17:45	2018-09-13 15:00 2018-09-16 03:00	BD1: 2018-09-13 18:49 BD2: 2018-09-15 18:17
Murphy	Grass	685	40.513 N 108.566 W	2018-09-01 01:43	2018-09-01 00:00 2018-09-03 00:00	M1: 2018-09-01 12:14 M2: 2018-09-02 11:26
Indian Valley	Understory	6310	40.192 N 108.201 W	2018-07-20 19:20	2018-07-20 18:00 2018-07-23 06:00	IV1: 2018-07-21 10:46 IV2: 2018-07-22 12:03
Hayden Pass	Understory	16,574	38.292 N 105.833 W	2016-07-08 23:53	2016-07-08 21:00 2016-07-12 21:00	HP1: 2016-07-12 02:29 HP2: 2016-07-12 04:18

* Times are in UTC.

3.2. Fire Perimeter Observation

To evaluate the model performance, we used fire perimeter data from the National Interagency Fire Center (NIFC). These parameters are derived from a variety of sources, including aerial surveys and field reports. The dataset is regularly updated and used by emergency responders and land managers to help determine the extent of active fire and burned areas. As active fire observations are being used to assess model output, it is essential to confirm that the observed data has a reliable timestamp. For this reason, we used the satellite-based VIIRS/NPP [18] 375 m Active Fire Data to cross-reference the timing of the NIFC perimeters. In cases where similar perimeters exist with different timestamps—sometimes separated by days—we selected only one perimeter for detailed analysis.

Figure 1 shows the fire perimeter from NIFC incident reports and the progression of the active fire areas as detected by VIIRS/NPP. In the Boone Draw case (Figure 1a), a grass fire, the fire rapidly spread from the ignition point detected at 17:45 UTC on September 13, moving over relatively flat terrain. The first perimeter is recorded at 00:49 UTC on 14 September 2018, indicating a northeast spread of the fire. This timing aligns closely with active fire detection from the satellite at 20:36 UTC on September 13 (the difference is less than the satellite revisit period). The fire's progression then slowed, with no further spread in the northeast boundary, indicating a possible fire suppression effort. The fire continued to spread to the northwest and southeast flanks at a slower rate. The second perimeter was recorded at 00:17 UTC on September 16. However, satellite observations showed that the fire reached the second perimeter by 20:18 UTC on September 14. This difference suggests that the NIFC perimeter timestamp was recorded well after the fire's actual arrival. Despite the inconsistency in the temporal evolution of the perimeters and satellite observation, their spatial alignment remains close.

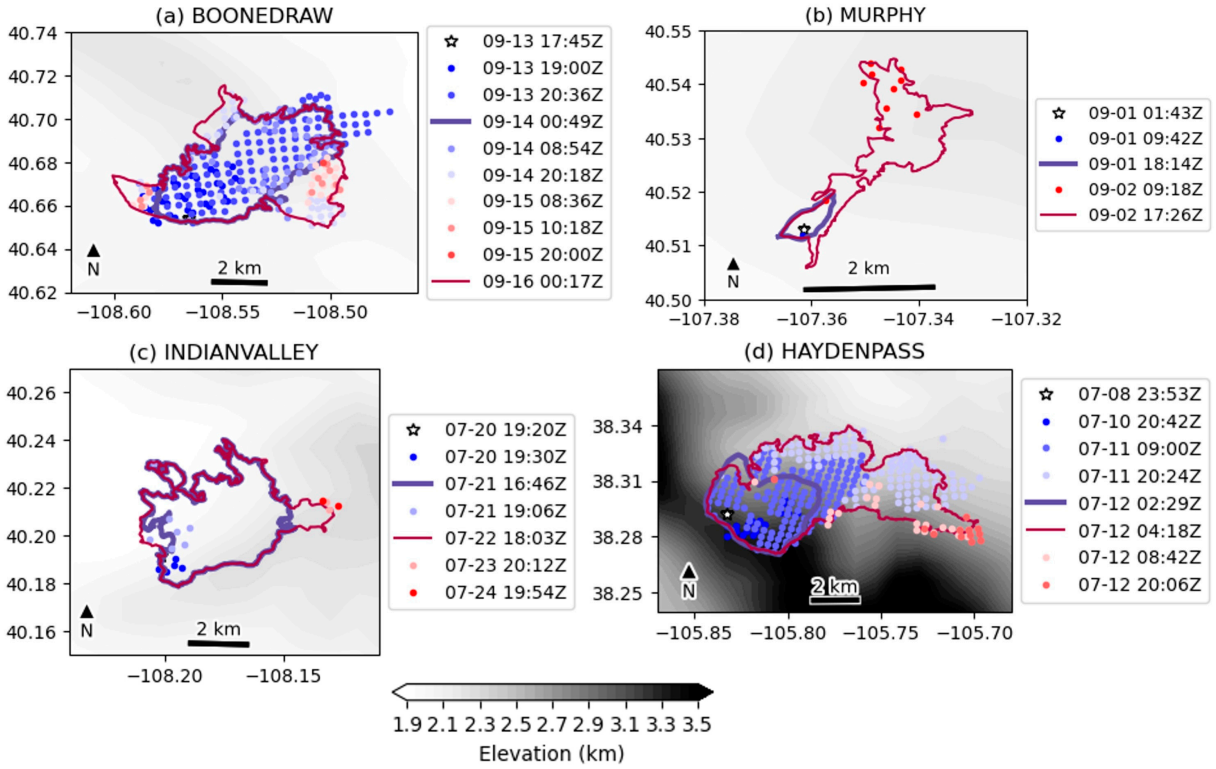

Figure 1. Footprint of active fire areas as reported by NIFC perimeters for (**a**) Boone Draw, (**b**) Murphy, (**c**) Indian Valley, and (**d**) Hayden Pass. The figures illustrate fire perimeters at different observation times (shown with colored lines), with fire detection points (stars) as reported in the incident reports, and active fire spots detected by VIIRS/NPP (colored dots). The background shading represents the topographic elevation. The times are in UTC. Each panel includes a 2 km scale bar and a North orientation arrow for geographic reference.

In the Murphy case (Figure 1b), another grass fire, two perimeter observations are available: 01:43 UTC on September 1 and 09:18 UTC on 2 September 2018. The recorded fire perimeter remained stable in all directions except toward the northeast, indicating containment or blocking of the fire spread within those boundaries. The spatial satellite observations are consistent with the perimeter data. However, as in the Boone Draw case, the satellite detection time suggests that the fire arrived at the second perimeter earlier, likely before 17:26 UTC on September 2, compared to the recorded perimeter timestamp. Therefore, for both cases, we used the satellite detection time for model evaluation. Additionally, we expect the model to overestimate fire spread, as fire suppression efforts are not accounted for in the model.

The Indian Valley and Hayden Pass fires (Figure 1c,d) are both surface fires influenced by canopy sheltering. The Indian Valley fire (Figure 1c) started at 19:20 UTC on 20 July 2018 and progressed in a northeast direction, with two perimeters recorded at 16:46 UTC on July 21 and 18:03 UTC on July 22. The comparison between the two perimeters suggests most of the fire front was inactive, likely due to containment efforts. Finally, the Hayden Pass (Figure 1d) fire, the largest fire simulated in our study, started at 23:53 UTC on 8 July 2016, with two perimeters recorded at 02:29 UTC and 04:19 UTC on July 12. Again for this case, the fire perimeter remained active only in the northwest direction between the two recorded perimeters, indicating containment of the fire. The fire progression seen by the satellite suggests that the timestamp of the first perimeter should be earlier than what is recorded.

In general, we observed a close agreement between the spatial shape of the perimeters and satellite retrievals of the active fire. In all cases, the fire perimeters remained stable

and inactive in some directions, suggesting containment between two timestamps in most directions, which is not captured by the model. Since fire containment is not included in the model, we expect the model to overestimate the fire spread. While the NIFC perimeters provide valuable spatial information, their timestamps may not always align accurately with actual fire progression. Therefore, for the Boone Draw and Murphy cases, we used the satellite time for model evaluation instead of the perimeter timestamp. By cross-referencing with VIIRS active fire data, we can improve our understanding of fire growth timing and ensure more reliable validation of the model's performance.

3.3. CFBM Experimeents

In our numerical experiments, CFBM calculates wind for fire spread using logarithmic interpolation (based on Equation (1)) with surface roughness derived from the atmospheric model. The default wind height in the WRF-Fire and CFBM namelist is 1 m, which can overestimate the spread rate for most fires. However, for the forested areas where atmospheric roughness length can be about 1 m, this approximation is unrealistic. For all cases, we conducted an experiment using the default model configuration, referred to as CTRL. For grass fire cases, we examined two approaches. We used Equation (4) to calculate the average wind at mid-flame height (OPT1), assuming the flame length extension ($H = H_F$) equals the fuel bed depth, and Equation (3), which assumes a variable flame length, determined using Byram's equation (OPT2). For partially and fully sheltered fire spread, a constant WAF value between 0.1 and 0.3 is typically used (see [25]). We conducted two experiments using constant values of 0.1 (C-0.1) and 0.2 (C-0.2).

3.4. Performance Metrics

We quantified the model performance using performance diagrams [26], which provide a comprehensive framework for evaluating the relationship between model predictions and observed fire spread. A performance diagram compares model accuracy against observed data by displaying four key contingency metrics: the Probability of Detection (POD = A/(A + C)) on the y-axis, the Success Ratio (SR = A/(A + B)) on the x-axis, the Critical Success Index (CSI = A/(A + B + C)) as solid curved lines, and bias levels (Bias = (A + B)/(A + C)) as dotted diagonal lines. These metrics are computed using the relationships among hits (A), false alarms (B), and misses (C). Note that CSI is equivalent to the similarity index (also known as the Jaccard index), which was used for fire area comparisons in the past (e.g., [9]).

In our analysis, we projected the NIFC fire perimeters onto the model grid by assuming a pixel represented active fire if its center was inside the observed perimeter. A grid point was classified as a hit (A) if the model correctly predicted fire where it was observed, as a false alarm (B) if the model predicted fire that was not observed, and as a miss (C) if the observed fire was not detected by the model. It should be noted that while the performance diagram provides an assessment of detection accuracy, false alarms, and prediction bias, it does not provide a comparison between the geometric similarity (e.g., the orientation of the fire spread) between the model and observations.

4. Results

4.1. Fire Spread Simulations

Figure 2 compares the observed fire perimeters from the NIFC dataset (solid blue line) with the modeled perimeters for the grass fire cases (Boone Draw and Murphy). We show results from the CTRL (solid black line), OPT1 (dashed blue line), and OPT2 (dashed black line) simulations. All the experiments reasonably captured the direction and magnitude of fire spread for the first Boone Draw perimeter (BD1, Figure 2a) at 00:49 UTC

on September 14, with the CTRL configuration slightly overestimating the spread. For the second perimeter (BD2, Figure 2b), compared against the satellite detection time (20:15 UTC on September 14), all models overestimated the observed perimeter. However, OPT1 and OPT2 showed smaller biases. This overestimation was particularly evident in areas where the fire front had remained stationary between BD1 and BD2. For the Murphy grass fire (Figure 2c,d), all models also overestimated the fire spread. In this case, the fire perimeter remained inactive in all directions except toward the northeast, where the simulated perimeter was closer to the observed one (Figure 2d). In both grass fire cases (BD1–BD2 and M1–M2), substantial portions of the observed fire perimeter remained unchanged between observation times, indicating containment that is not represented in the model. In both cases, since the model does not account for fire suppression efforts or barriers to fire spread (e.g., roads or rivers), these factors contributed to the overestimation of the fire spread. Our experiments further indicate that the difference between OPT1 and OPT2 simulations is small. This implies that, for our case study, variations in Equation (4) for flame-height estimates have a minor effect on the WAF, suggesting the model is relatively insensitive to flame-height assumptions under these conditions.

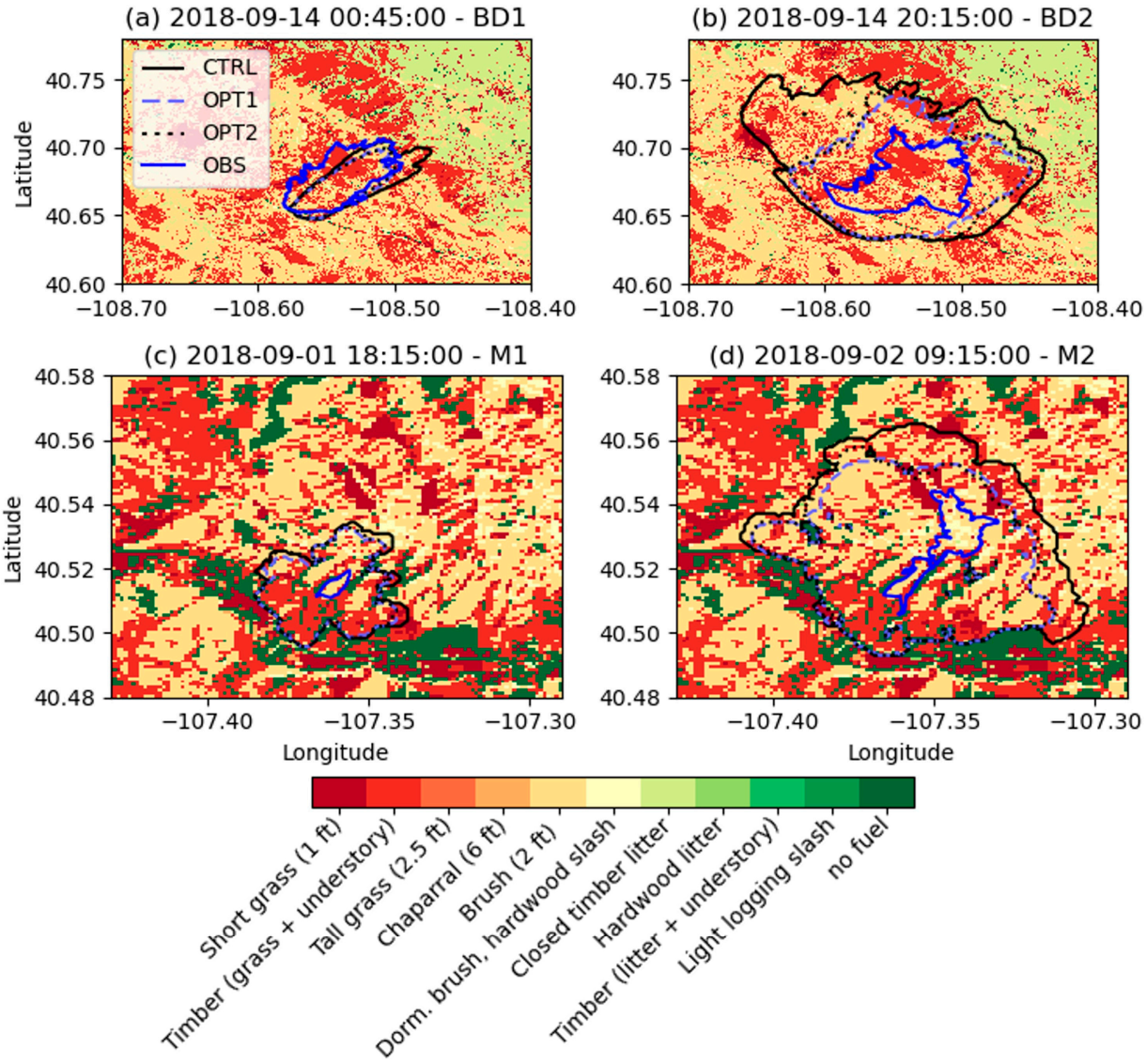

Figure 2. Comparison of observed and simulated fire perimeters for two grass fire cases: Boone Draw (**a**,**b**) and Murphy (**c**,**d**). Panels (**a**,**b**) correspond to the first (BD1) and second (BD2) perimeters for

Boone Draw, while (**c**,**d**) correspond to the first (M1) and second (M2) perimeters for Murphy. The observed NIFC perimeters (solid blue line) are shown alongside modeled perimeters from the CTRL (solid black), and with WAF for unsheltered fire spread OPT1 (blue dashed) and OPT2 (black dashed). The background shading represents the underlying fuel types. For the second perimeter time comparisons, the observed fire perimeters are compared with satellite detection time at 20:18 UTC on September 14 for BD1 and 09:18 on September 2 for M2.

In Figure 3, we show the results for the sheltered fires, for which we conducted simulations with the standard CFBM (CTRL) model and two constant WAF configurations (C-0.1 and C-0.2), corresponding to dense and open stands of fully sheltered canopy [25]. Indian Valley fire (Figure 3a,b) is over an area with predominantly grass and understory fuel, while Hayden Pass (Figure 3c,d) is over an area with predominantly timber litter and understory. Both sets of simulations were conducted in complex forested terrains where wind attenuation by canopy is expected to influence fire spread. For both Indian Valley and Hayden pass fire, all the models overestimated the fire perimeter runs. However, both the C-0.1 and C-0.2 simulations produced more realistic results, indicating that even a constant WAF can better represent sub-canopy wind attenuation.

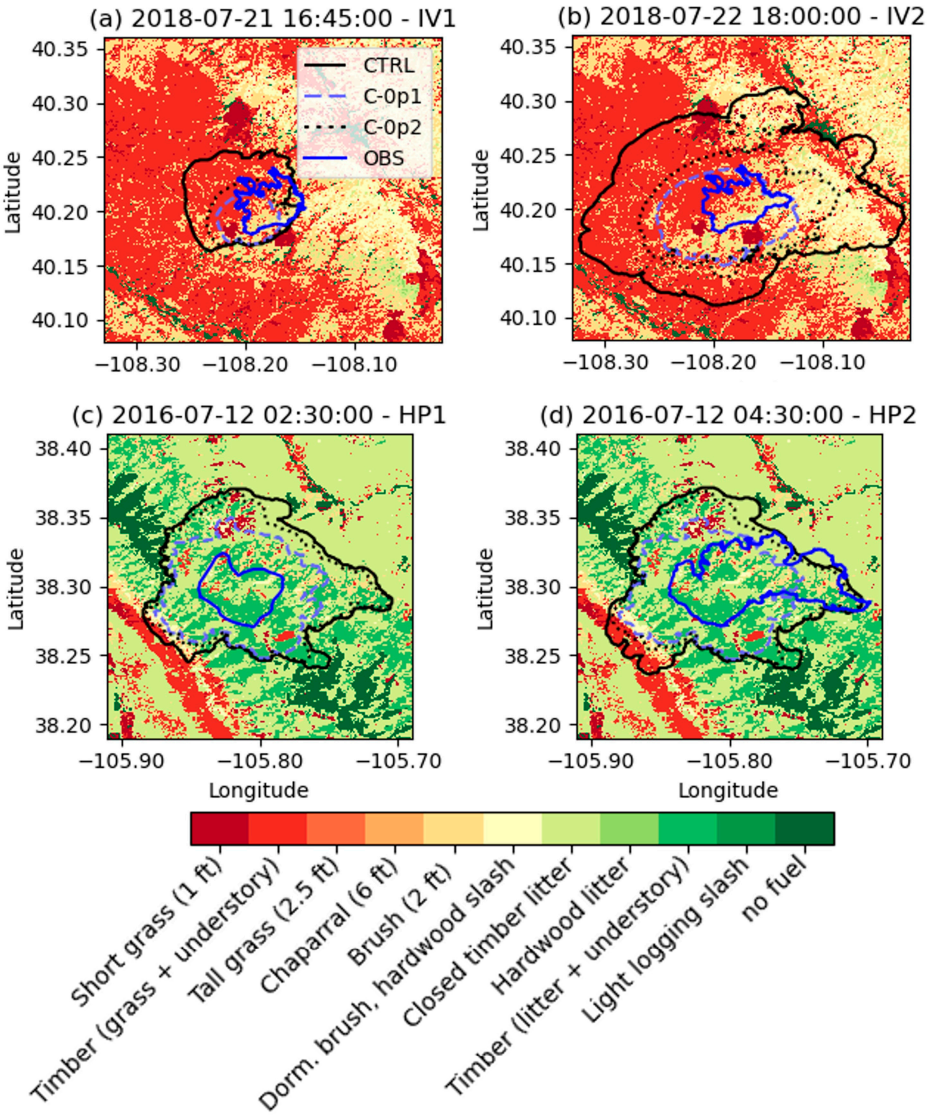

Figure 3. Comparison of observed and simulated fire perimeters for two sheltered fire cases: Indian Valley (**a**,**b**) and Hayden Pass (**c**,**d**). Panels (**a**,**b**) correspond to the first (IV1) and second (IV2) perimeters

for Indian Valley, while (**c**,**d**) correspond to the first (HP1) and second (HP2) perimeters for Hayden Pass. The observed NIFC perimeters (solid blue line) are shown alongside modeled perimeters from the CTRL (solid black), C-0.1 (blue dashed), and C-0.2 (black dashed) simulations. The background shading represents the underlying fuel types.

4.2. Performance Analysis

The performance diagrams in Figure 4 quantify the predictive accuracy of fire perimeter simulations for all four cases. In the Boone draw case (Figure 4a), the control simulation showed a lower bias compared to the WAF simulations (OPT1 and OPT2) for the first perimeter (BD1), which underpredicted the fire spread. Nevertheless, the success ratio for the CTRL run is lower than the WAF simulations because of higher false alarms (see also Figure 2a). For the second perimeter time (BD2), all the models overestimated the fire spread; however, the WAF cases showed lower bias and better success ratios.

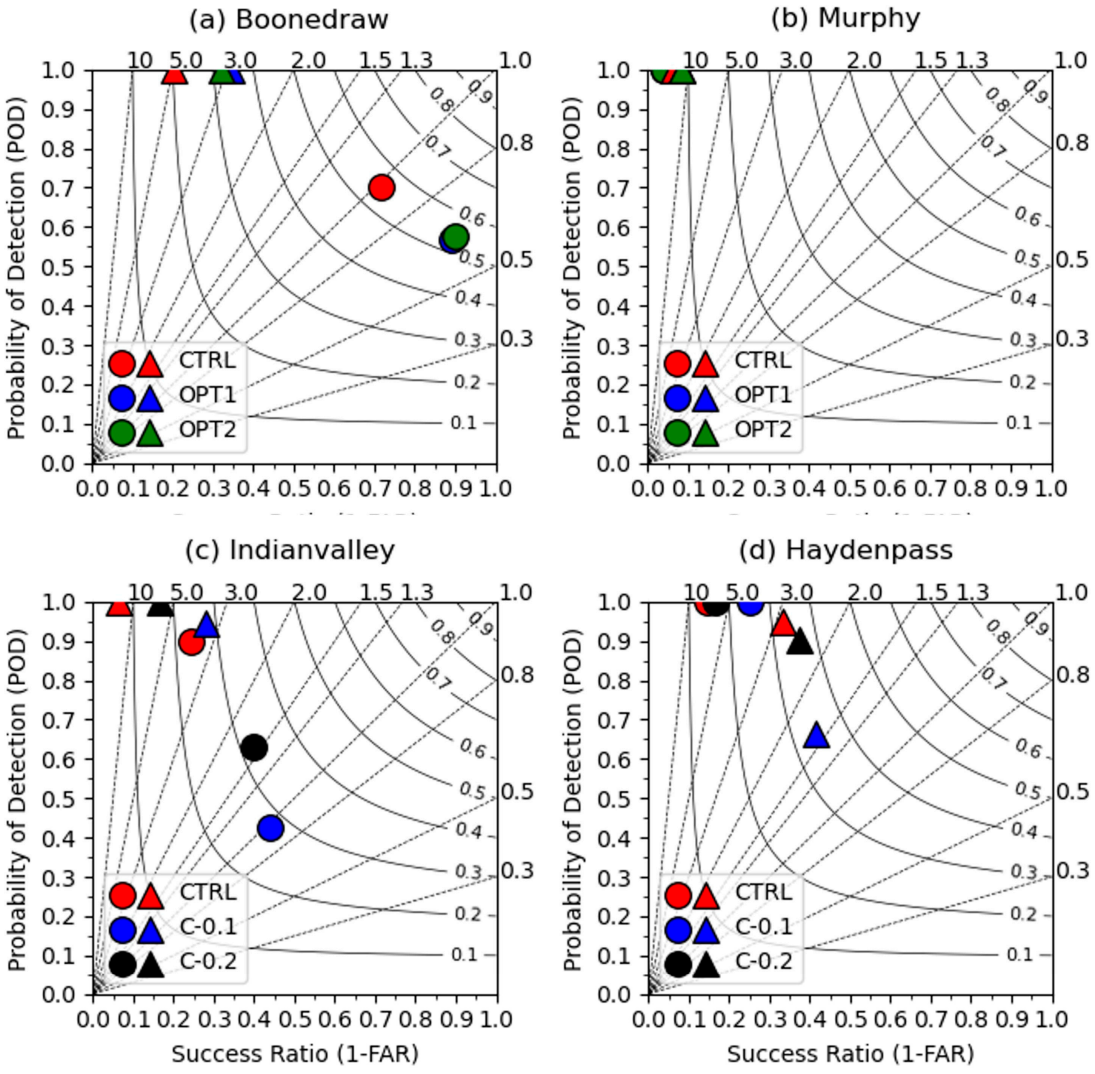

Figure 4. Performance diagram for fire perimeter simulations for four cases: (**a**) Boonedraw, (**b**) Murphy, (**c**) Indian Valley, and (**d**) Hayden Pass. The solid curved lines represent the Critical Success Index (CSI), while the diagonal dotted lines indicate bias levels. Circles represent comparisons with the first perimeter (BD1, M1, IV1, and HP1), while triangles represent the second perimeter (BD2, M2, IV2, HP2), based on simulation times shown in Figures 2 and 3 for each case.

In the Murphy case (Figure 4b), all simulations (CTRL, OPT1, and OPT2) exhibited high POD but very low SR, clustering near the upper-left corner of the diagram for both

perimeters (M1 and M2). This indicates a strong tendency to overpredict fire spread (see Figure 2), especially for smaller fires such as this case, as reflected by the high bias levels.

In the Indian Valley case (Figure 4c), the CTRL simulation showed a higher POD and bias than C-0.1 and C-0.2 for the first perimeter (IV1). For the second perimeter (IV2), all the cases had a high POD but the CTRL case had a much lower SR and higher bias. The Hayden Pass case (Figure 4d) showed a similar trend to Indian Valley. For both cases, it can be seen that C-0.1 showed a lower bias, but C-0.2 showed a better SR.

Across all four cases, the control simulations consistently exhibited high POD but suffered from overprediction, as evidenced by low SR and high bias values. The WAF implementation generally improved the SR by reducing false alarms, thereby lowering the bias. Among the optimized approaches, configurations like OPT2 for Boonedraw and C-0.2 for Indian Valley and Hayden Pass provided the most balanced results, achieving higher CSI values and closer alignment with lower bias levels.

5. Conclusions

In this study, we examined different wind parameterizations for use in fire spread modeling in the Community Fire Behavior Model (CFBM). The current model available in CFBM is based on logarithmic interpolation using the atmospheric roughness length, while the new WAF implementations rely on fuel bed depth height for unsheltered fires and a prescribed value for sheltered surface fires within the canopy. The fuel bed depth is available at a higher resolution, providing a more accurate representation of the fuels compared to the roughness length from the atmospheric model. For the first time in this context, we compared the resulting fire perimeters to the NIFC perimeter observations, interpreting them alongside VIIRS satellite-based active fire detections.

For sheltered (grass) fires, the WAF-based approach generally improved fire perimeter predictions in terms of success ratio and bias compared to the control simulations. This improvement was particularly evident in reducing the overestimation of fire spread, which is common when the default approach with fixed wind heights and logarithmic interpolation is used. Among the model configurations, OPT1, which assumes a constant flame length, and OPT2, which uses an empirical equation to diagnose the flame length, both performed closely. The results were similar for OPT1 (constant flame length) and OPT2 (empirical flame-height diagnosis), indicating that, in these cases, the model (Equation (4)) is relatively insensitive to flame-height assumptions. For sheltered fires, simulations employing constant WAF values C-0.1 and C-0.2 (representing dense and open canopy conditions) produced more realistic results than the current approach, even though there was no canopy density data available to calculate an accurate WAF constant. These results highlight the importance of integrating fuel-specific parameters to represent the midflame winds.

The comparison of NIFC perimeters and VIIRS active fire detections showed a close agreement in spatial patterns. However, there are temporal inconsistencies, with the timestamps of NIFC perimeters often lagging the satellite detections. These discrepancies underscore the need for more consistent observational data to support improved model evaluation. Furthermore, fire prediction inherently involves multiple sources of error, emphasizing the need for broader validation across diverse spatial domains and fire cases. Fuel characterization (e.g., fuel moisture) remains a key area of uncertainty, as it significantly influences fire behavior modeling. Future studies should incorporate a larger sample of fire events to identify potential weaknesses and areas for improvement.

In summary, this study demonstrates the effectiveness of WAF implementation in improving fire spread predictions for both sheltered and unsheltered fire cases. Additionally, the new implementation simplifies the modeling process by eliminating the need for users to specify a wind height parameter, thereby enhancing the objectivity and operational

utility of the CFBM. Nonetheless, further research is necessary to refine fuel characterizations, address potential biases, and assess model performance across a wider range of fire conditions.

Author Contributions: Conceptualization and methodology, M.E. and P.A.J.y.M.; formal analysis and visualization, M.E.; data curation, A.D.; writing—original draft preparation, M.E.; writing—review and editing, all the authors; visualization, M.E.; funding acquisition, P.A.J.y.M. All authors have read and agreed to the published version of the manuscript.

Funding: This research was funded by NOAA under Award No. NA22OAR4590514-T1-01. The simulations were conducted on Derecho (https://doi.org/10.5065/qx9a-pg09), which is provided by NSF NCAR's Computational and Information Systems Laboratory (CISL) and sponsored by the U.S. National Science Foundation.

Institutional Review Board Statement: Not applicable.

Informed Consent Statement: The study is not involving humans.

Data Availability Statement: The CFBM is available as open-source code in Zenodo (https://zenodo.org/records/13357368, accessed on 20 May 2024) and in this git repository: https://github.com/NCAR/fire_behavior, accessed on 20 May 2024. WRF is available at https://github.com/wrf-model, accessed on 20 May 2024.

Acknowledgments: This material is based upon work supported by the NSF National Center for Atmospheric Research, which is a major facility sponsored by the U.S. National Science Foundation under Cooperative Agreement No. 1852977.

Conflicts of Interest: The authors declare no conflicts of interest. The funders had no role in the design of this study; in the collection, analyses, or interpretation of data; in the writing of the manuscript; or in the decision to publish the results.

Abbreviations

The following abbreviations are used in this manuscript:

CFBM	Community Fire Behavior Model
CSI	Critical Success Index
HRRR	High-Resolution Rapid Refresh
ICM	Improved Canopy Model
NIFC	National Interagency Fire Center
NWP	Numerical Weather Prediction
POD	Probability of Detection
SR	Success Ratio
VIIRS	Visible Infrared Imaging Radiometer Suite
WAF	Wind Adjustment Factors
WRF	Weather Research and Forecasting

References

1. Clark, T.L.; Coen, J.; Latham, D. Description of a coupled atmosphere–fire model. *Int. J. Wildland Fire* **2004**, *13*, 49–63.
2. Coen, J.L.; Cameron, M.; Michalakes, J.; Patton, E.G.; Riggan, P.J.; Yedinak, K.M. WRF-Fire: Coupled Weather–Wildland Fire Modeling with the Weather Research and Forecasting Model. *J. Appl. Meteorol. Climatol.* **2013**, *52*, 16–38.
3. Mandel, J.; Beezley, J.D.; Kochanski, A.K. Coupled atmosphere-wildland fire modeling with WRF 3.3 and SFIRE 2011. *Geosci. Model Dev.* **2011**, *4*, 591–610. [CrossRef]
4. Muñoz-Esparza, D.; Kosović, B.; Jiménez, P.A.; Coen, J.L. An Accurate Fire-Spread Algorithm in the Weather Research and Forecasting Model Using the Level-Set Method. *J. Adv. Model. Earth Syst.* **2018**, *10*, 908–926. [CrossRef]
5. Rothermel, R.C. *A Mathematical Model for Predicting Fire Spread in Wildland Fuels*; Intermountain Forest & Range Experiment Station, Forest Service; U.S. Department of Agriculture: Ogden, UT, USA, 1972.

6. Alexander, M.E.; Cruz, M.G. Interdependencies between flame length and fireline intensity in predicting crown fire initiation and crown scorch height. *Int. J. Wildland Fire* **2011**, *21*, 95–113.
7. Finney, M.A.; Grumstrup, T.P. Effect of flame zone depth on the correlation of flame length with fireline intensity. *Int. J. Wildland Fire* **2023**, *32*, 1135–1147. [CrossRef]
8. Jiménez, P.A.; Muñoz-Esparza, D.; Kosović, B. A High Resolution Coupled Fire–Atmosphere Forecasting System to Minimize the Impacts of Wildland Fires: Applications to the Chimney Tops II Wildland Event. *Atmosphere* **2018**, *9*, 197. [CrossRef]
9. Shamsaei, K.; Juliano, T.W.; Roberts, M.; Ebrahimian, H.; Kosovic, B.; Lareau, N.P.; Taciroglu, E. Coupled fire-atmosphere simulation of the 2018 Camp Fire using WRF-Fire. *Int. J. Wildland Fire* **2023**, *32*, 195–221. [CrossRef]
10. Jimenez y Munoz, P.A.; Frediani, M.; Eghdami, M.; Rosen, D.; Kavulich, M.; Juliano, T.W. The Community Fire Behavior Model for coupled fire-atmosphere modeling: Implementation in the Unified Forecast System. *Geosci. Model Dev. Discuss.* **2024**, 1–30. [CrossRef]
11. Skamarock, W.C.; Klemp, J.B.; Dudhia, J.; Gill, D.O.; Zhiquan, L.; Berner, J.; Wang, W.; Powers, J.G.; Duda, M.G.; Barker, D.M.; et al. *A Description of the Advanced Research WRF Model Version 4.3*; National Center for Atmospheric Research (NCAR): Boulder, CO, USA, 2021. [CrossRef]
12. Byram, G.M. Combustion of forest fuels. In *Forest Fire: Control and Use*; Davis, K.P., Ed.; McGraw-Hill Book Company: New York, NY, USA, 1959; pp. 61–89.
13. Hung, W.; Campbell, P.C.; Moon, Z.; Saylor, R.; Kochendorfer, J.; Lee, T.R.; Massman, W. Evaluation of an In-Canopy Wind and Wind Adjustment Factor Model for Wildfire Spread Applications Across Scales. *J. Adv. Model. Earth Syst.* **2024**, *16*, e2024MS004300. [CrossRef]
14. Mallia, D.V.; Kochanski, A.K.; Urbanski, S.P.; Mandel, J.; Farguell, A.; Krueger, S.K. Incorporating a Canopy Parameterization within a Coupled Fire-Atmosphere Model to Improve a Smoke Simulation for a Prescribed Burn. *Atmosphere* **2020**, *11*, 832. [CrossRef]
15. Massman, W.J.; Forthofer, J.M.; Finney, M.A. An improved canopy wind model for predicting wind adjustment factors and wildland fire behavior. *Can. J. For. Res.* **2017**, *47*, 594–603. [CrossRef]
16. Baughman, R.G.; Albini, F.A. Estimating Midflame Windspeeds. In Proceedings of the Sixth Conference on Fire and Forest Meteorology, Seattle, WA, USA, 22–24 April 1980; pp. 88–92.
17. Finney, M.A. *FARSITE, Fire Area Simulator--Model Development and Evaluation*; U.S. Department of Agriculture, Forest Service, Rocky Mountain Research Station: Ogden, UT, USA, 1998.
18. Schroeder, W.; Oliva, P.; Giglio, L.; Csiszar, I.A. The New VIIRS 375 m active fire detection data product: Algorithm description and initial assessment. *Remote Sens. Environ.* **2014**, *143*, 85–96. [CrossRef]
19. Benjamin, S.G.; Weygandt, S.S.; Brown, J.M.; Hu, M.; Alexander, C.R.; Smirnova, T.G.; Olson, J.B.; James, E.P.; Dowell, D.C.; Grell, G.A.; et al. A North American Hourly Assimilation and Model Forecast Cycle: The Rapid Refresh. *Mon. Weather. Rev.* **2016**, *144*, 1669–1694. [CrossRef]
20. Thompson, G.; Eidhammer, T. A Study of Aerosol Impacts on Clouds and Precipitation Development in a Large Winter Cyclone. *J. Atmos. Sci.* **2014**, *71*, 3636–3658.
21. Jiménez, P.A.; Dudhia, J.; González-Rouco, J.F.; Navarro, J.; Montávez, J.P.; García-Bustamante, E. A Revised Scheme for the WRF Surface Layer Formulation. *Mon. Weather Rev.* **2012**, *140*, 898–918. [CrossRef]
22. Iacono, M.J.; Delamere, J.S.; Mlawer, E.J.; Shephard, M.W.; Clough, S.A.; Collins, W.D. Radiative forcing by long-lived greenhouse gases: Calculations with the AER radiative transfer models. *J. Geophys. Res. Atmos.* **2008**, *113*, D13103.
23. Dudhia, J. Numerical Study of Convection Observed during the Winter Monsoon Experiment Using a Mesoscale Two-Dimensional Model. *J. Atmos. Sci.* **1989**, *46*, 3077–3107. [CrossRef]
24. Tewari, M.; Chen, F.; Wang, W.; Dudhia, J.; Lemone, A.; Mitchell, E.; Ek, M.; Gayno, G.; Węgiel, W.; Cuenca, R. Implementation and Verification of the unified NOAH Land Surface Model in the WRF Model. In Proceedings of the 20th Conference on Weather Analysis and Forecasting/16th Conference on Numerical Weather Prediction, Seattle, WA, USA, 12–16 January 2004.
25. Andrews, P.L. Modeling Wind Adjustment Factor and Midflame Wind Speed for Rothermel's Surface Fire Spread Model. RMRS-GTR-266. 2012. Available online: https://www.fs.usda.gov/treesearch/pubs/39729 (accessed on 6 March 2024).
26. Roebber, P.J. Visualizing Multiple Measures of Forecast Quality. *Weather Forecast.* **2009**, *24*, 601–608. [CrossRef]